

Determination of Working Pressure for Airport Runway Rubber Mark Cleaning Vehicle Based on Numeric Simulation

Haojun Peng^{1,*}, Zhongwei Wu¹, Jinbing Xia¹, Bolin Dong¹, Yuntao Peng², Linghe Wang³, Xingxing Ma³ and Wei Shen³

Abstract: In this paper, numeric simulations are performed for three dimension models built according to actual surface cleaner in airport runway rubber mark cleaning vehicle using ANSYS FLUENT software on the basis of previous research finished by the authors. After analyzing the simulated flow fields under different standoff distances between nozzle outlet and runway surface and different discharge pressures at nozzle outlet, the relationships of normal stress and shear stress at striking point to outlet pressure and standoff distance are obtained. Finally, the most appropriate discharge pressure at nozzle outlet for the studied surface cleaner model is found, and this will provide theoretical basis for future rubber mark cleaning process in airports and equipment model selection in subsequent design of airport runway rubber mark cleaning vehicles.

Keywords: Runway cleaning, surface cleaner, numeric simulation, nozzle pressure, pump model selection.

1 Introduction

Severe friction between tire and runway during landing and takeoff will cause some rubber layer on tire surface fallen and adhered on runway surface. This process repeats over and over, adhered rubber layer on runway surface becomes thicker and thicker and leads to decreased friction coefficient and a prolonged running distance during landing, which may make a bad influence on flight safety.

Once the friction factor is decreased below the lowest limit required by regulation [Jiang, Zhang, Wen et al. (2013)], a cleaning process to remove adhered rubber mark should be taken. Nowadays, most civil airports in China use high pressure waterjet airport runway rubber mark cleaning vehicle to fulfill this process. Fig. 1 shows the schematic structure of surface cleaner used. The body of surface cleaner is a 304 stainless steel shell, on top of whose center a high pressure rotary coupling is installed. Four spraying rods are mounted evenly at coupling's end with each high pressure nozzle installed at the end and driven to rotate during cleaning. On top of shell, at a certain distance from axis, there is a vacuum suction port. Cleaned solid particles and waste water will be sucked out of shell and collected

¹ School of Mechanical Engineering, Hefei University of Technology, Hefei, China.

² Fire Detachment in Xi'an Xianyang International Airport Co., Ltd., Xianyang, China.

³ Security Service Co. Ltd., Xi'an Xianyang International Airport, China West Airport Group, Xianyang, China.

* Corresponding Author: Haojun Peng. Email: peng.gusi@hfut.edu.cn.

in sewage tank for further treatment. Between lower end of shell and ground, a small gap is set to let air flowing in. But for consideration of decreasing vacuum pump's power consumption and preventing huge noise generated during cleaning from leaking out, this gap is usually wrapped by two or three layers of nylon brush strip to prevent excessive leakage.

Pressure, standoff distance and rotation speed are the three key parameters in rubber mark cleaning process. The influences of standoff distance and rotation speed on cleaning effect have been studied in our previous work [Peng and Zhang (2018)]. At then, the influence of working pressure on interior flow field in surface cleaner, and the relationship of pressure to normal striking stress and shear stress has not acquired. Thus, the optimal working pressure is remained unknown. But in fact, working pressure should be first determined in equipment design and operation. Since once structure of nozzle is chosen, most key parameters, such as needed driving power, dimension and manufacturing cost, even the loading capacity and length of required truck chassis, are all related to it.

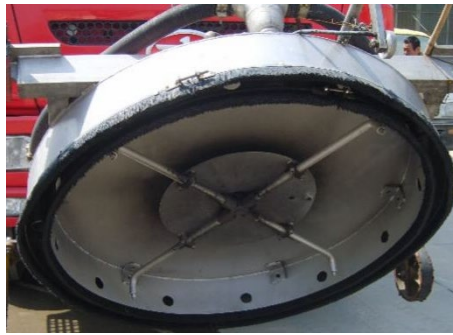


Figure 1: Structure of surface cleaner [Peng and Zhang (2018)]

At present, working pressure is chosen according to previous experiences, or parameters of similar products made by other manufacturers. There has seldom quantitative analysis. This will not only lead to waste of equipment performance and rising of manufacturing and operation cost, but once carelessness occurs during cleaning and working pressure exceeds threshold value, it is very easy to damage runway surface. Because of this, it is urgently needed to simulate and quantitatively analyze the interior flow field in surface cleaner during operation, and choose the most appropriate operation pressure on basis of study results. This will also provide the manufacturers with credible bases to minimize the required parameters and manufacturing cost.

2 Description of problem

Continuous waterjet flows out of nozzle orifice will reach supersonic speed under normal cleaning parameters [Xue, Huang, Chen et al. (1998)]. Once entering ambient atmosphere, such a high speed waterjet certainly generates violent turbulence, stirs surrounding air and makes great noise. Large quantity of water mist is produced during waterjet entraining air and impacting to ground, combined with high speed rotation of spraying rods and nozzles, makes it impossible to observe cleaning effect directly. So, each surface cleaner employs a stainless steel shell to isolate noise and water mist from leaking out. This simple structure surely improves working conditions during cleaning, but the nontransparent shell makes

direct examination and parameter measurement impossible. Considering the obstruction caused by high speed waterjet, diffusing water mist and the nontransparent shell in conjunction with the complicate turbulent multi-phase flow field generated by both water and air inside the shell, the feasible research method can only be the numeric simulation combining with field tests.

Decades have passed since high pressure waterjet technology was successfully and practically applied in industry. Convincible conclusions and data about the single waterjet have been acquired on basis of experimental analyses and numeric simulations. Sun [Sun (1992)] provided an empirical equation to calculate the dynamic pressure at jet axis and its distribution in different section faces. Labus [Labus (1995)], Summers [Summers (1995)] and many other researchers all pointed out that the whole waterjet structure can be basically divided into initial section, basic section and dissipation section. Their conclusions stated that only the basic section of waterjet can be used for industrial cleaning, descaling and surface polishing, while the initial section is fit for waterjet cutting, and the dissipation section is normally used in dust elimination since the jet has been severely diffused in this part. Tikhomirov et al. [Tikhomirov, Babanin, Petukhov et al. (1992)] discussed the interaction procedure between waterjet droplet and target material. They measured the relation of jet pressure to jet striking time at center of jet impacting area and summarized the relationship of jet's striking force on target surface with standoff distance during waterjet cutting under different working pressures and nozzle sizes on the basis of experiment data.

Since the late 1990s, further researches have been carried out to investigate the interaction between single high pressure waterjet and target material with the help of numeric simulation. Leu et al. [Leu, Meng, Geskin et al. (1998)] set up a mathematic model for waterjet cleaning process and pointed out that the cleaning effect can only be seen if the shear stress produced by water droplet during impacting on target is equal to or large than the fatigue limit of target material. Researches done by Welker et al. [Welker, Nagarajan and Newberg (2005)] showed that the elimination process of solid particles adhered on target surface was mainly related to shear stress generated by waterjet striking on target surface. Yang et al. [Yang, Zhou and Liu (2008)] calculated the velocity field and pressure field of waterjet in atmosphere produced by different nozzles under several working conditions by means of numeric simulation. Guha et al. [Guha, Barron and Balachandar (2011)] combined experiment with numerical simulation and studied relationship of volume fraction decay and velocity of water phase at centerline to standoff distance using free waterjet with a relatively low speed (about 80~200 m/s). They compared results with experimental data published by Rajaratnam N., Albers C. and found a good coincidence. Li et al. [Li, Wang, Zhu et al. (2013)] simulated the impact procedure of 350 ~ 700 m/s ultra-high speed waterjet onto high strength steel plate during abrasive waterjet descaling and analyzed the transferring procedure of impact energy to ductile material, the relationships of erosion cavity's volume and material removing efficiency to different impacting variables and yield strength of target material.

But for flow field in multi-beam waterjet applications, seldom research and literature can be found. Reason for this mainly lies in the rare application of multi-beam waterjet. Most industrial cleaning and cutting using high pressure waterjet can be accomplished by single waterjet beam. Even if there has an application using multi-beam waterjet, such as

descaling in steel plants, the waterjets are separated to relatively large distance and are fixed to stationary positions. But for surface cleaner applied in airport runway rubber mark cleaning vehicle, its complicate working conditions make the research be totally different. To reduce the power of the vacuum pump, lower edge of surface cleaner shell is neither a fully-opened structure nor a fully-closed one. There is a nylon brush strip installed around the cleaner shell's lower edge to shelter the gap between edge and ground and this makes the interior of cleaner shell a semi-closed cavity. During rubber mark cleaning process, the nozzles are rotated along with spraying rods driven by hydraulic motor and a rotating flow field is formed. At the same time, the intake air from interstices between bristles, the outflow of mixture comprised of water, air and cleaned solid debris at entrance of vacuum suction port on top of cleaner's shell and the inner surface of shell, plus the forward speed of loaded truck, combine together to form a distorted flow field, which is seldom seen in other applications. Few research and literature can be searched relating to this kind flow field with high rotation speed in a semi-closed vacuum cavity. The only related research can be found partially done by Li et al. [Li, Xue and Zhou (2007)] in their study about ultra-high pressure waterjet rust cleaning. They investigated velocity distribution of waterjet under 200 MPa, gave the distribution of pressure and fluid velocity on jet impacting surface, put forward the relationship between impacting force on plate surface and standoff distance, and finally, discussed the optimization of waterjet's parameters. But in their research, they assumed that the rotation speed of spraying rod is ZERO. Meanwhile, there has a much more small volume of water needed in ultra-high pressure waterjet rust cleaning process (normally below 15 L/min) since most of this kind of cleaning is fulfilled on fixed site. So there is no requirement of vacuum suction air from the gap between lower edge of cleaner's shell and surface to drain the cleaned substance. So they omitted the influence of jet stream rotation and intake air to cleaning effect and characteristics of flow field. Thus, their study can only act as a partial reference. In order to gain more precise conclusions, as many working conditions encountered in actual cleaning process as possible should be considered during our study on surface cleaner in airport runway rubber mark cleaning vehicle.

In summary, we should find the optimal and most appropriate working pressure for surface cleaner under the pretense of 30mm standoff distance and 1100 rpm rotation speed gained in previous research.

3 Set-up of simulation

Fig. 2 shows the geometry model drawn according to actual surface cleaner. The main body is a cylindrical shell with 1050 mm diameter and 185 mm height. A 6 mm air intake gap is located between lower edge of shell and ground, which is equivalent to the flow area in brush bristles' interstice. A 100 mm cylindrical outlet is mounted on top of shell and 400 mm away from axis acting as the vacuum suction port. Four 22 mm outer diameter spraying rods are mounted symmetrically at center on top shell plate, each has a 1 mm cylindrical nozzle at the end.

The interior of model is the actual computational domain. The model for calculation is built in Solidworks through intersection and then imported to Fluent 17.0. Mesh model using tetrahedral element is shown in Fig. 3, in which the meshes in inner fluid volume and on

bottom surface are hidden for clear illustration.

3.1 Selection of turbulence model

The most frequently used turbulence models in Fluent are mainly the $k-\varepsilon$ model and $k-\omega$ model. Our previous research shows that the inner flow field within surface cleaner shell is in a severely turbulent state. Under the combined situation affected by severely turbulent flow field within surface cleaner shell, violent momentum and energy exchange between waterjet stream and surrounded atmosphere, the relatively high speed intake air from the lower gap and the influence of high rotation speed of spraying rod to jet's trajectory, the $k-\omega$ model is much more appropriate for this simulation than $k-\varepsilon$ model.

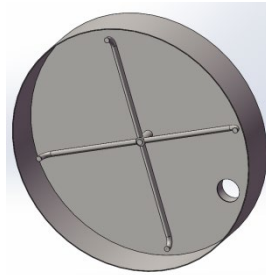


Figure 2: Geometry model of surface cleaner [Peng and Zhang (2018)]

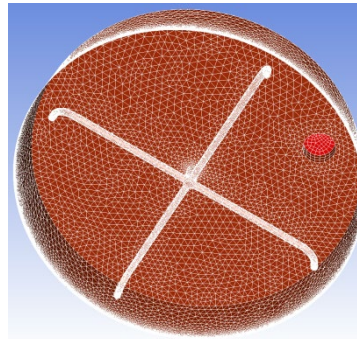


Figure 3: Mesh model after inner fluid volume and bottom surface is hidden

Turbulence viscosity μ_t is introduced in standard $k-\omega$ model, which is defined as following:

$$\mu_t = \alpha \frac{\rho k}{\omega} \tag{1}$$

k equation and ω equation of *SST* $k-\omega$ model are listed as following:

$$\frac{\partial(\rho k)}{\partial t} + \frac{\partial(\rho k u_i)}{\partial x_i} = \frac{\partial}{\partial x_j} \left(\Gamma_k \frac{\partial k}{\partial x_j} \right) + G_k - Y_k + S_k \tag{2}$$

$$\frac{\partial(\rho\omega)}{\partial t} + \frac{\partial(\rho\omega u_i)}{\partial x_i} = \frac{\partial}{\partial x_j} \left(\Gamma_\omega \frac{\partial\omega}{\partial x_j} \right) + G_\omega - Y_\omega + D_\omega + S_\omega \quad (3)$$

In Eq. (2) and Eq. (3), G_k is the turbulent kinetic energy generated by average velocity gradients, G_ω is the turbulent kinetic energy generated by ω equation. Γ_k and Γ_ω is the diffusivity coefficient of k and ω generated by turbulence respectively. Y_k and Y_ω is the dissipation of k and ω due to turbulence respectively. S_k and S_ω is the source term defined by the user. σ_k and σ_ω is the turbulence Prandtl number for k and ω equation, and D_ω is cross diffusion term and is defined as following,

$$D_\omega = 2(1 - F_t)\rho\sigma_{\omega,2} \frac{1}{\omega} \frac{\partial k}{\partial x_j} \frac{\partial \omega}{\partial x_j} \quad (4)$$

where the blending function F_t is defined as $F_t = \tanh(\arg_1^4)$

$$\text{where } \arg_1^4 = \min \left[\max \left(\frac{\sqrt{k}}{C_\mu \omega y}, \frac{500\nu}{y^2 \omega} \right), \frac{4\rho\sigma_{\omega,2}k}{CD_{k\omega}y^2} \right]$$

Here y is defined as the normal distance to wall and $CD_{k\omega}$ is the positive portion of the cross diffusion term [Kummitha (2017)].

3.2 Selection of multiphase flow model

This simulation is an air-water two-phase model. According to our previous works, the formerly applied Mix model is selected again as the multiphase flow model.

The continuity equation of Mix model is given as following,

$$\frac{\partial}{\partial t}(\rho m) + \nabla \cdot (\rho_m \vec{v}_m) = \dot{m} \quad (5)$$

Here, \vec{v}_m is the mass-averaged velocity given by $\vec{v}_m = \frac{\sum_{k=1}^n \alpha_k \rho_k \vec{v}_k}{\rho_m}$, and ρ_m is the mixture

density given by $\rho_m = \sum_{k=1}^n \alpha_k \rho_k$. In above expressions, α_k is the volume fraction of phase k .

The momentum equation of Mix model is given as following,

$$\begin{aligned} \frac{\partial}{\partial t}(\rho_m \vec{v}_m) + \nabla \cdot (\rho_m \vec{v}_m \vec{v}_m) = & -\nabla p + \nabla \cdot [\mu_m (\nabla \vec{v}_m + \nabla \vec{v}_m^T)] \\ & + \rho m \vec{g} + \vec{F} + \nabla \cdot \left(\sum_{k=1}^n \alpha_k \rho_k \vec{v}_{dr,k} \vec{v}_{dr,k} \right) \end{aligned} \quad (6)$$

where n is number of phases; \vec{F} is the volume force; μ_m is the mixture viscosity and given

by $\mu_m = \sum_{k=1}^n \alpha_k \mu_k$; $\vec{v}_{dr,k}$ is the drift velocity of phase k and calculated by $\vec{v}_{dr,k} = \vec{v}_k - \vec{v}_m$.

3.3 Boundary conditions

High pressure rotating joint and spraying rods in most rubber mark cleaning equipment are forced to rotate by hydraulic motor, there is no need of tangential component of jets' reaction force. So the end of spraying rod is normally set to be vertical to ground. Hence, only the vertical impacting jet stream is considered in this simulation.

Normally, there are two types of nozzle installed at the end of spraying rod, which are the fan nozzle and multi fine cylindrical hole nozzle. To simplifying simulation, all nozzles are converted to equivalent nozzle with single cylindrical hole. Four nozzles are set to be pressure inlet ranging from 50 MPa to 90 MPa at an interval of 5 MPa. Orifice of vacuum suction pipe is set to be pressure outlet working at absolute pressure of 0.08 MPa (relatively pressure is -0.02 MPa) and remained constant in all simulation cases. Gap between lower edge of surface cleaner shell and ground is set to be speed inlet, the intake air velocity is calculated according to the bleed air rate of vacuum pump under selected driving speed and given vacuum degree.

4 Discussion

4.1 Flow field in surface cleaner's shell

Fig. 4 shows the liquid water phase distribution on bottom surface in calculated domain (that is to say, the runway surface) in same scale under 30 mm standoff distance and 1100 rpm rotation speed, which are acquired in previous study, but different pressures. We can see that under 50 MPa pressure, jet's velocity is relatively small, percentage of liquid water on bottom surface is relatively small too, so color representing distribution of liquid water phase deviates to blue end, which means a smaller content. With the increase of pressure, waterjet's velocity is increased from 316.6 m/s at 50 MPa to 424.7 m/s at 90 MPa, percentage of liquid water phase on bottom surface is also increased. The area with brighter color in each drawing is also enlarged. But whether the pressure is low or high, region with relatively high content of liquid water phase is around the striking point beneath each nozzle outlet. Meanwhile, obvious clockwise tails can be observed in each flow field, which are caused by rotation of spraying rods. Besides, ends of four clockwise fluid flow tails are all slightly deflected to lower right, which is more obvious after pressure exceeding 65 MPa. This is mainly caused by the suction flow in suction port.

Fig. 5 shows velocity distribution on section plane through nozzle axis in same scale under 30 mm standoff distance and 1100 rpm rotation speed, but different pressure. We can see that velocity at nozzle outlet is the maximum value in each graph. Along with the gradually enlarged distance from nozzle outlet, velocity of waterjet is gradually decreased. There has an obvious initial section and basic core section in each velocity field. Meanwhile, a larger velocity at top of each diagram near cleaner's shell can be found compared with bottom of each diagram, which means the place farther away from shell wall. This reflects the obvious wall-attachment effect existing in flow field in surface cleaner.

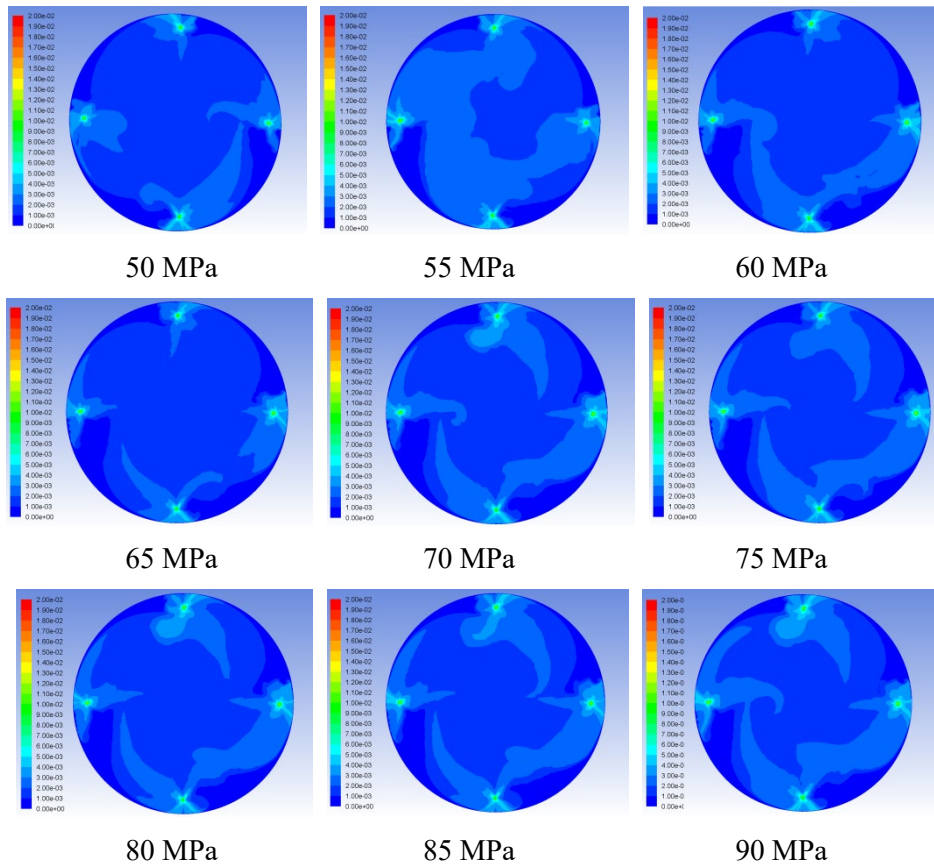
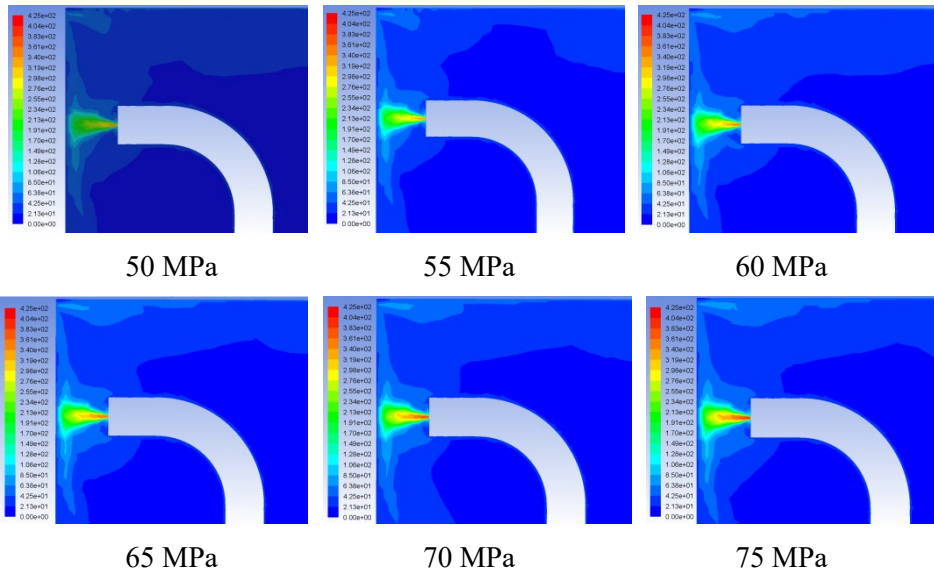


Figure 4: Liquid water phase distribution on bottom surface in same scale under 30 mm standoff distance, 1100 rpm rotation speed and difference pressure



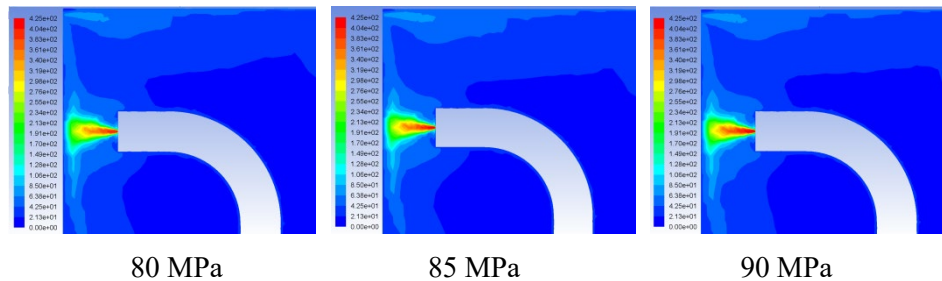


Figure 5: Velocity distribution on section plane through nozzle axis in same scale under 30 mm standoff distance, 1100 rpm rotation speed and different pressure

4.2 Selection of working pressure

Generally, when nozzle diameter and standoff distance are set to fixed value, the greater outlet pressure is, the greater jet's speed is, and the greater kinetic energy of jet striking on ground is, which leads to a larger normal stress at impacting point. On the other hand, if pressure and nozzle diameter are kept unchanged and only the standoff distance is changed, then the larger distance makes a smaller striking force. There is an opposite relationship between these two variables, since the jet's kinetic energy is exhausted more by atmosphere because of the larger distance, so the jet's kinetic energy is decreased gradually along with the distance from nozzle outlet. Fig. 6 and Fig. 7 show the relationship of maximum normal stress at striking point to pressure and standoff distance respectively. They all verify the above basic relationships.

In Fig. 6, it is very interesting to find that the maximum normal stress on striking point is basically linear to pressure. Among these, when standoff distance lies between 15 mm to 25 mm, the maximum normal stress declines by a big margin. For instance, under normally used pressure of 75 MPa during cleaning, when the standoff distance is 15 mm, 20 mm and 25 mm, the maximum normal stress is 2.23 MPa, 1.24 MPa and 0.75 MPa respectively. The maximum stress at 25 mm is reduced to 33.6% of that value at 15 mm. If the standoff distance is larger than 25 mm, although the maximum stress is still getting smaller when standoff distance gets larger, but the decreasing degree is not as serious as that when standoff distance is smaller than 25 mm. If observing the curve with single standoff distance, the greater the distance is, the gradually smaller increment of maximum stress at striking point for same pressure increment is. This can be seen from the decreasing slope of curve along with the increasing standoff distance, which means that one will get half the results with twice the effort if standoff distance is greater than optimal range and hoping to improve cleaning effect only by increasing working pressure.

When pressure is kept unchanged, the maximum normal stress at striking point is reduced sharply at beginning with the increasing distance, slope of curve is much bigger. After distance is greater than 25 mm, slope of curve is evidently reduced. These can all be seen in Fig. 7.

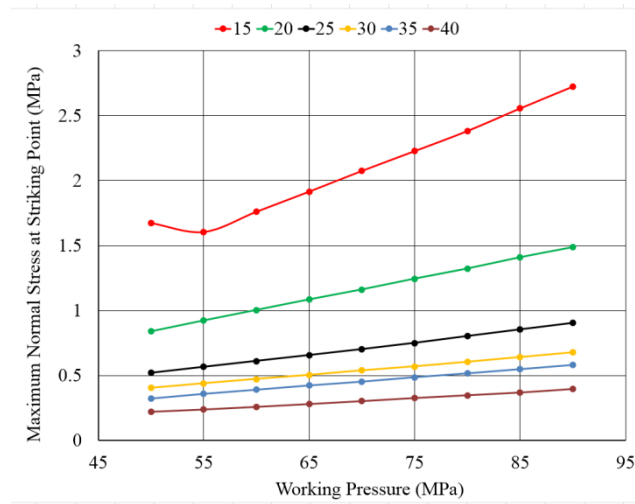


Figure 6: Relationship between maximum normal stress at striking point and pressure

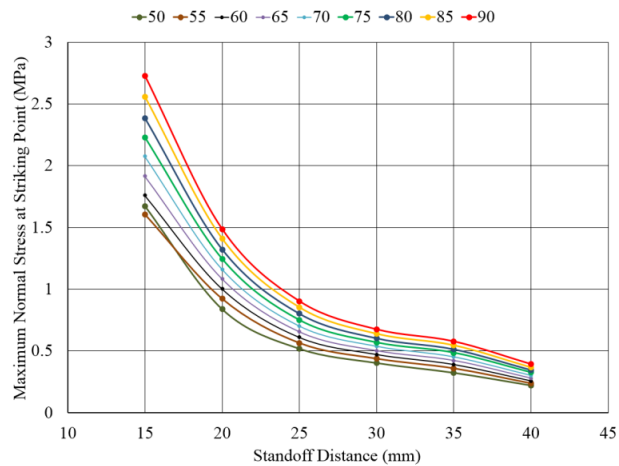


Figure 7: Relationship between maximum normal stress at striking point and standoff distance

Fig. 8 and Fig. 9 show the relationship of maximum shear stress at striking point to pressure and standoff distance respectively. These two relations are similar to those displayed in Fig. 6 and Fig. 7. The biggest difference is that the maximum shear stress at striking point is not ideally linear to pressure under certain distance. The possible reasons for this may attribute to rotation of spraying rod, suction air flow on top surface or intake air from bottom gap.

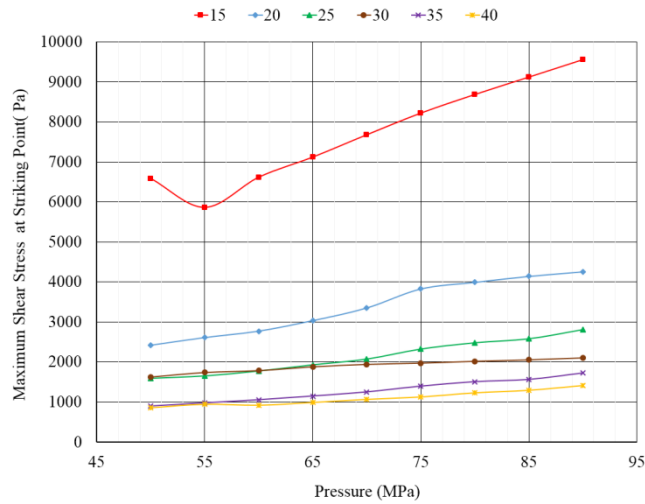


Figure 8: Relationship between maximum shear stress at striking point and outlet pressure

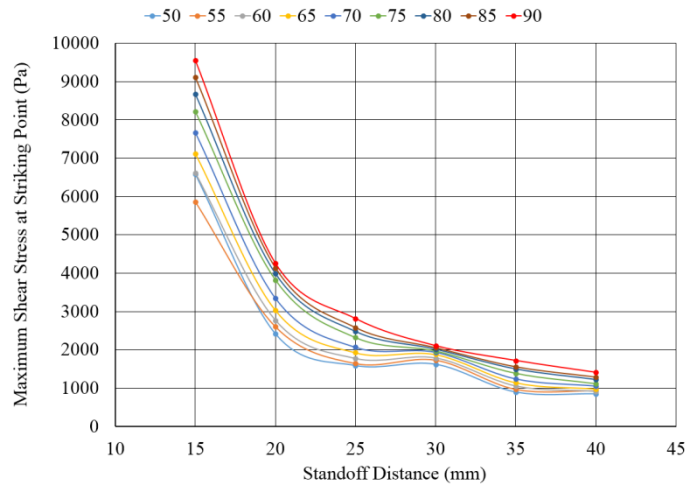


Figure 9: Relationship between maximum shear stress at striking point and standoff distance

If there is no influence of suction air, intake air and rotation speed, the flow field of single jet should be symmetrical to nozzle axis. But when considering the influence of rotation, though the actual standoff distance from outlet to actual striking point is varied in different nominal standoff distance, but calculations show that this variation is very small and can be omitted. The main reason for this is the very short period time of waterjet flowing in air from outlet to ground. In this millisecond order interval, there is an order of magnitude difference between tangential flowing distance of jet and the nominal standoff distance, so the influence of rotation can be ignored. Tab. 1 shows the actual standoff distance corresponding to different nominal distance under 75 MPa pressure and 1100 rpm rotation

speed. So, after eliminating the rotation speed, the relation of maximum shear stress at striking point to pressure under certain standoff distance is mainly affected by suction air flow on top surface and intake air flow in bottom gap. Within these two factors, bottom gap is much more near to nozzle outlet and the intake air speed is much larger than that of suction air, the intake air flow in bottom gap should be dominant.

Table 1: Actual standoff distance corresponding to nominal distance under 75 MPa and 1100 rpm

Nominal standoff distance (mm)	15	20	25	30	35	40
Estimated tangential flowing distance (mm)	1.5	2.0	2.7	3.5	4.6	5.2
Estimated actual standoff distance (mm)	15.1	20.1	25.1	30.2	35.3	40.3

The high speed waterjet generated by nozzle is utilized in rubber mark cleaning on runway surface. The ideal cleaning effect is a thoroughly cleaned runway surface without any damage. If merely considering from the view of cleanness, the higher the outlet pressure is and the smaller the standoff distance is, the better cleaning effect is. But normally, when cleaning is needed, thickness of adhered rubber layer is not very large. High speed rotating four nozzles in cleaner will complete cleaning process instantly and runway surface will be exposed directly under waterjet. So, normal stress at striking point generated by waterjet should not exceed certain value, otherwise the direct impacting high speed waterjet will make dents on runway surface after rubber layer is removed, that is to say, damage to runway surface is occurred.

According to “Specifications for Airport Cement Concrete Pavement Design” (MH/T 5004-2010) [Jiang, Qin, Yang et al. (2010)], which should be obeyed during design and construction of civil airport runway surface, flexural tensile strength of concrete runway in civil airport should not be smaller than 4.5 MPa, and the cement strength grade should be at least 42.5 and 52.5 corresponding to this requirement. The maximum characteristic of concrete is that its tensile strength is only 1/10 to 1/20 portion of its compression strength and the tensile strength normally lies in range of 2.5 to 2.6 MPa (Tab. 4.1.3-2) [Zhao, Xu, Huang et al. (2010)].

Zha et al. [Zha (2015); Xie (2015)] and other researchers concluded that cavitation mechanism holds dominant position among all fracture mechanisms of rubber under high pressure waterjet. Researches to investigate the relationship of impacting pressure on target surface by cavitation waterjet to that of continuous waterjet finished by Li [Li (2009)] shows that the impacting pressure of cavitation waterjet is normally 8.6 to 124 times that of continuous waterjet.

During cleaning, the initially continuous waterjet with supersonic velocity will exchange momentum and energy with surrounding air during flowing in air and be broken gradually. The broken jet stream surely involves some air bubbles and an immature cavitation waterjet is formed. At this time, even calculated under 4.5 MPa flexural tensile strength of surface material and relatively smaller magnification, the waterjet will probably damage runway

surface after adhered rubber mark is cleaned if stagnation pressure at striking point exceeds the range of 0.4 to 0.5 MPa. Looking back to Fig. 6 and Fig. 8, we can find that, within the whole pressure range of 50 to 90 MPa, the normal stress values at striking point under 15 mm, 20 mm and 25 mm standoff distances for studied 1mm cylindrical nozzle all exceed 0.5 MPa, so these three standoff distances should be avoided during cleaning process. And for 30 mm and 35 mm standoff distances, the waterjet is safe to runway surface provided that the outlet pressure is less than 80 to 85 MPa; while to the 40 mm distance, the waterjet is safe to runway within the whole pressure range of 50 to 90 MPa.

On the basis of above analyses, considering the rubber mark cleaning process using high pressure waterjet on runway surface is mainly dependent on the shear stress in adhered rubber layer generated by waterjet. Once the generated shear stress exceeds shear strength of rubber layer with multi-layer structure, cracks will emerge and expand, and at last, rubber layer begins to break into pieces. So, the greater shear stress at striking point is, the better cleaning effect and efficiency are. According to Fig. 8, Fig. 9 and our previous research, under the optimized 30mm standoff distance and 1100rpm rotation speed, 75 MPa is the most appropriate pressure at nozzle outlet and should be selected as top priority.

4.3 Test verification

Xi'an Xianyang International Airport, China West Airport Group, has utilized waterjet technology for runway cleaning since 2008. The studied surface cleaner in this research belongs to the rubber mark cleaning vehicle owned by it. Based on the parameters gained by the authors, we set the standoff distance to 30 mm and rotation speed to 1100 rpm and test cleaning effect and efficiency under different working pressure. Data acquired from tests shows that if pressure is lower than 75 MPa, cleaning speed is decreased significantly, fallen down from 3~3.5 m/min at 75 MPa to about 2 m/min at 65 MPa, and some thicker rubber layer cannot be cleaned thoroughly in single cleaning process and needs two, even three cleaning. This surely decreases cleaning efficiency. On the other hand, if pressure exceeds 75 MPa, cleaning efficiency for thicker rubber layer is also increased. But if cleaning area with thinner rubber layer, the vehicle moving speed should be increased to avoid possible damage on runway surface. And this is very hard to handle for operator working in night, since he cannot observe runway surface clearly in dark night only by his naked eyes. So, considering all aspects involving runway cleaning, 75 MPa is a most appropriate pressure value to select.

5 Conclusion

In this paper, based on the author's previous researches, the same model is adopted to analyze the inner flow field within surface cleaner applied in airport runway rubber mark cleaning vehicle under different standoff distances and outlet pressures. After analyzing and summarizing the relationships of normal stress and shear stress at striking point to standoff distance and outlet pressure, the most appropriate outlet pressure of 75 MPa for studied equipment is obtained. This result provides a more reliable numeric basis for high pressure pump model selection and is helpful to avoid blindness encountered in previous model selection and actual operation.

Acknowledgement: Many thanks should be given to Dejun Liu and Hefei Xingliang Machinery Co., Ltd., who provided many help in this research, including supplying CAD file and measuring operation conditions during their project to supply maintenance for high pressure waterjet airport runway rubber cleaning vehicle in Xi'an Xianyang International Airport.

References

- Chen, Y.** (1991): *Turbulence Model*. Press of University of Science and Technology of China.
- Anglani, F.; Barry, J.; Dekkers, W.** (2017): Development and validation of a stationary water-spray cleaning system for concentrated solar thermal (CST) reflectors. *Solar Energy*, vol. 155, pp. 574-583.
- Fu, S.; Dong, L.; Yuan, H.** (2014): Numerical simulation and analysis of velocity field in horizontal screw centrifuge based on euler multiphase model. *Chemical Industry and Engineering Progress*, vol. 33, pp. 36-42.
- Guha, A.; Barron, R. M.; Balachandar, R.** (2011): An experimental and numerical study of water jet cleaning process. *Journal of Materials Processing Technology*, vol. 211, pp. 610-618.
- Guo, L.** (2002): *Dynamics of Two-Phase and Multi-Phase Flow*. Xi'an Jiaotong University Press.
- Han, Y.; Li, J.** (2012): Selection of fluid jet nozzle under vacuum based on fluent simulation and analysis. *Vacuum*, vol. 49, pp. 19-23.
- Jiang, C.; Qin, H.; Yang, S.; Sun, Y.; Li, N.** (2010): *MH/T 5004-2010, Specifications for Airport Cement Concrete Pavement Design*. Civil Aviation Administration of China.
- Jiang, C.; Zhang, Y.; Wen, S. et al.** (2013): *MH 5001-2013, Aerodrome Technical Standards*. Civil Aviation Administration of China.
- Kummitha, O. R.** (2017): Numerical analysis of hydrogen fuel scramjet combustor with turbulence development inserts and with different turbulence models. *International Journal of Hydrogen Energy*, vol. 42, pp. 6360-6368.
- Labus, T. J.** (1995): *Fluid Jet Technology: Fundamentals and Applications*. WJTA.
- Leu, M. C.; Meng, P.; Geskin, E. S.; Tismeneskiy, L.** (1998): Mathematical modeling and experimental verification of stationary waterjet cleaning process. *Manufacturing Science Engineering, Trans ASME*, vol. 120, no. 3, pp. 571-579.
- Li, F.** (2009): *Study on Vessel Cleaning Technology of Cavitation Waterjet (Ph.D. Thesis)*. Harbin Engineering University, China.
- Li, J.; Xue, S.; Zhou, Q.** (2007): Numerical simulation of ultra high pressure pure water jet rust removal machine. *Engineering Journal of Wuhan University*, vol. 40, pp. 48-57.
- Li, W.; Wang, J.; Zhu, H.; Huang, C.** (2013): On ultrahigh velocity micro-particle impact on steels - a single impact study. *Wear*, vol. 305, pp. 216-227.
- Peng, H.; Zhang, P.** (2018): Numerical simulation of high speed rotating waterjet flow field in a semi enclosed vacuum chamber. *Computer Modeling in Engineering & Sciences*,

vol. 114, no. 1, pp. 59-73.

Sharif, M. A. R.; Guo, G. (2007): Computational analysis of supersonic turbulent boundary layers over rough surfaces using the $k-\omega$ and the stress- ω models. *Applied Mathematical Modelling*, vol. 31, pp. 2655-2667.

Summers, D. A. (1995): *Waterjetting Technology*. E & FN SPON.

Sun, J. (1992): *Waterjet Cutting Technology*. Press of China University of Mining and Technology.

Tikhomirov, R. A.; Babanin, V. F.; Petukhov, E. N.; Starikov, I. D.; Kovalev, V. A. (1992): *High-Pressure JetCutting*. ASME.

Welker, R.; Nagarajan, R.; Newberg, C. (2005): Getting clean parts and getting parts clean. *Contamination and ESD Control in High-Technology Manufacturing*, pp. 195-275.

Xie, R. (2015): *Fracture Mechanism of Waste Radial Tyre Rubber under Ultra-High Pressure Water Jet Impact (Ph.D. Thesis)*. Hefei University of Technology, China.

Xue, S.; Huang, W.; Chen, Z.; Fan, Y; Peng, H. et al. (1998): *Technology and Application of High Pressure Waterjet*. China Machine Press.

Yang, G.; Zhou, W.; Liu, F. (2008): Flow field simulation of high pressure waterjet nozzle based on fluent. *Journal of Lanzhou University of Technology*, vol. 34, pp. 49-52.

Zha, H. (2015): *Cavitation and Desulfurization Mechanism of Ground Tire Rubber under Ultra-High Pressure Water Jet Impacting Radial Tire (Ph.D. Thesis)*. Hefei University of Technology, China.

Zhao, J.; Xu, Y.; Huang, X. et al. (2010): *GB 50010-2010, Code for Design of Concrete Structures*. Ministry of Housing and Urban-Rural Development of the People's Republic of China.